Research Article

Mohamed Khalil Yousef Soliman, Ahmed Soliman Doghish, Amr Hosny Hashem*, Mostafa Abdel-Maksoud, Walaa Ahmed El-Dakroury, Abdulaziz Alamri, Hossam Ebaid, Mohamed Sayed Hasanin, and Ebrahim Saied*

Novel trimetallic (TiO_2–MgO–Au) nanoparticles: Biosynthesis, characterization, antimicrobial, and anticancer activities

https://doi.org/10.1515/gps-2025-0007
received October 12, 2024; accepted February 25, 2025

Abstract: Trimetallic nanoparticles have garnered significant attention due to their promising biological activities. In this study, the aqueous extract of banana peel was utilized as a reducing and stabilizing agent for the green synthesis of novel trimetallic titanium dioxide–magnesium oxide–gold nanoparticles (TiO_2–MgO–Au NPs). The biosynthesized nanoparticles were spherical, with an average size of 55 nm as observed by transmission electron microscopy and 70 nm based on dynamic light scattering measurements. Antimicrobial tests revealed that the nanoparticles exhibited minimum inhibitory concentration values of 500 $\mu g \cdot mL^{-1}$ against *Bacillus subtilis* and *Escherichia coli*, 250 $\mu g \cdot mL^{-1}$ against *Pseudomonas aeruginosa* and *Candida albicans*, and 125 $\mu g \cdot mL^{-1}$ against *Staphylococcus aureus*. The nanoparticles demonstrated significant antibiofilm activity, inhibiting methicillin-resistant *S. aureus* biofilm formation by 86.8% at 250 $\mu g \cdot mL^{-1}$ and by 25.1% at 15.62 $\mu g \cdot mL^{-1}$. The MTT assay showed strong cytotoxic effects on MCF-7 and HepG2 cancer cells, with the lowest IC_{50} value of 11.09 ± 1.02 $\mu g \cdot mL^{-1}$ observed in MCF-7 cells. Additionally, ELISA results confirmed that TiO_2–MgO–Au NPs enhanced the activation of caspase-8 while reducing the levels of VEGFR-2. In conclusion, the biosynthesized TiO_2–MgO–Au NPs showed significant antimicrobial, antibiofilm, and anticancer potential, particularly against breast cancer cells, indicating their potential as a novel therapeutic agent.

Keywords: trimetallic nanoparticles, antimicrobial activity, anticancer activity, biosynthesis, fruit peels, therapeutic agent

*** Corresponding author: Amr Hosny Hashem,** Botany and Microbiology Department, Faculty of Science, Al-Azhar University, Nasr City, 11884, Cairo, Egypt, e-mail: amr.hosny86@azhar.edu.eg
*** Corresponding author: Ebrahim Saied,** Botany and Microbiology Department, Faculty of Science, Al-Azhar University, Nasr City, 11884, Cairo, Egypt, e-mail: hema_almassry2000@azhar.edu.eg
Mohamed Khalil Yousef Soliman: Botany and Microbiology Department, Faculty of Science, Al-Azhar University, Nasr City, 11884, Cairo, Egypt, e-mail: Mohamed.k.yousef@azhar.edu.eg
Ahmed Soliman Doghish: Department of Biochemistry, Faculty of Pharmacy, Badr University in Cairo, Badr City (BUC), Cairo, 11829, Egypt; Biochemistry and Molecular Biology Department, Faculty of Pharmacy (Boys), Al-Azhar University, Nasr City, 11231, Cairo, Egypt, e-mail: ahmed_doghish@azhar.edu.eg
Mostafa Abdel-Maksoud: Botany and Microbiology Department, College of Science, King Saud University, Riyadh, Saudi Arabia, e-mail: mabdmaksoud@ksu.edu.sa
Walaa Ahmed El-Dakroury: Department of Pharmaceutics and Industrial Pharmacy, Faculty of Pharmacy, Badr University in Cairo (BUC), Badr City, Cairo, 11829, Egypt, e-mail: Walaa.ahmed2@buc.edu.eg
Abdulaziz Alamri: Biochemistry Department, College of Science, King Saud University, Riyadh, Saudi Arabia, e-mail: abalamri@ksu.edu.sa
Hossam Ebaid: Department of Zoology, College of Science, King Saud University, P.O. Box 2455, Riyadh, 11451, Saudi Arabia, e-mail: habdrabou@ksu.edu.sa
Mohamed Sayed Hasanin: Department of Polymer and Biomaterials Science, West Pomeranian University of Technology in Szczecin, Al. Piastow 45, 70-311, Szczecin, Poland, e-mail: Sido_sci@yahoo.com

1 Introduction

Antibiotics are highly effective in protecting against a wide range of bacterial infections. However, one strategy bacteria use to enhance their resistance to antibiotics is mutation, leading to the emergence of multidrug-resistant (MDR) species and significantly diminishing the therapeutic efficacy of antibiotics. Concerns about the rise of antibiotic resistance are growing as bacteria actively develop and adapt their defense mechanisms against conventional antibiotics [1]. Furthermore, bacteria have evolved defense mechanisms against several inhibitors, such as the production of biofilms. Biofilms, composed of abiotic or biotic materials, are formed by live microorganisms that establish a strong attachment to the surface they colonize [2,3]. The substances released by the bacteria in the biofilm mediate

this interaction [4,5]. Moreover, bacteria's resistance to well-known antimicrobial drugs is caused by the biofilm matrix surrounding their cells. Therefore, many researchers are increasingly focusing on developing non-traditional antibiotics, including innovative nano-antibiotic compounds, to combat microorganism resistance [6,7]. Undoubtedly, creating new compounds capable of eliminating and preventing bacterial proliferation through innovative mechanisms is the solution to these challenges [8].

Chemotherapy, radiation therapy, and surgery improve cancer outcomes but have significant side effects. Nausea, exhaustion, hair loss, infertility, and secondary malignancies can result after chemotherapy. Radiation therapy can lead to skin irritation, fatigue, organ damage, and an increased risk of developing secondary malignancies. Surgical procedures can cause bleeding, infection, deformity, and psychological discomfort. These treatments are beneficial, but they emphasize the need for balanced approaches that regard the patient's well-being and continued research toward safer treatments [9]. Therefore, the primary goal of research in this field is to develop new methods or anti-cancer drugs that offer superior efficacy, minimal toxicity, excellent biocompatibility, and the ability to degrade naturally.

Nanotechnology is rapidly emerging as a crucial field, driving significant advancements in pharmaceutical delivery, bioavailability, imaging, and treatment while considering all relevant factors. Additionally, it effectively reduces the negative consequences associated with these procedures [10]. The use of nanoparticles as anticancer drugs offers multiple advantages. It can enhance the stability and longevity of the distribution of medications [11]. Nanoparticles can be precisely delivered to selectively target cancer cells, minimizing damage to healthy tissues. Nanoparticles can overcome the problem of multiple drug resistance by avoiding the P-glycoprotein efflux pump. Furthermore, they can deliver multiple therapeutic drugs simultaneously, facilitating the use of combination therapy. Specific stimuli can activate nanoparticles with advanced sensing capabilities to precisely release their payloads at the targeted site. This precise distribution strategy enhances the efficacy of treatment and reduces the negative side effects. Furthermore, nanoparticles can be designed to overcome drug resistance and improve drug solubility and loading efficiency. Nanoparticles possess unique attributes that make them an ideal platform for cancer therapy, including enhanced efficacy and improved safety [12,13].

Among different nanosized materials, MgO and TiO_2 nanoparticles have recently been thoroughly explored for their powerful anticancer activities. Various studies have demonstrated that minuscule nanoparticles composed of metal oxides could selectively target and eradicate cancer cells, even in very minute concentrations [14]. MgO and TiO_2 nanoparticles exhibit anticancer properties due to their capability to produce reactive oxygen species (ROS), which can trigger oxidative stress and apoptosis in tumor cells. The nanoparticles exhibited the capacity to disrupt the mitochondrial membrane. In addition, the nanoparticles can specifically gather in cancer cells, reducing harm to healthy cells [15].

Many inorganic NPs have antibacterial characteristics, including Ag, Au, Cu, CuO, Se, TiO_2, and ZnO [16–21]. Along with the other inorganic NPs, zinc oxide nanoparticles (ZnONPs) have received a lot of attention due to their affordable, easy-to-prepare nature that is safe for both humans and animals [22,23]. TiO_2NPs, biofabricated using *Staphylococcus aureus*, exhibit remarkable antibacterial and antibiofilm properties against various bacterial species, including *Bacillus subtilis* and *Escherichia coli* [24]. These nanoparticles are also extensively used in the production of medical supplies [25]. According to researchers, gold nanoparticles may prevent *S. aureus* and *Pseudomonas aeruginosa* from forming biofilms [26].

Multimetallic nanoparticles, composed of two or more different metallic elements, have emerged as promising multifunctional agents with both antimicrobial and anticancer properties [27–30]. These nanoparticles exploit the synergistic effects of the constituent metals to disrupt bacterial cell membranes, inhibit microbial enzymes and metabolic processes, and generate ROS that trigger oxidative stress [28]. This multi-pronged antimicrobial action allows trimetallic nanoparticles to be effective against a broad spectrum of pathogens, including drug-resistant strains [31]. Simultaneously, trimetallic nanoparticles can selectively target cancer cells by exploiting differences in cellular uptake, disrupting mitochondrial function, and triggering apoptotic pathways. The versatile design of trimetallic nanoparticles enables the tuning of their physicochemical properties to maximize antimicrobial efficacy while preserving their ability to target and destroy cancer cells [28]. This dual functionality makes trimetallic nanoparticles attractive candidates for applications in antimicrobial coatings, wound dressings, and targeted cancer therapeutics, where their multifunctional nature can be leveraged to address pressing clinical challenges. This study aimed to utilize banana peel extract for the green biosynthesis of novel trimetallic (TiO_2–MgO–Au) nanoparticles for the first time and to evaluate their antimicrobial and anticancer activities.

2 Materials and methods

2.1 Materials

Banana peels that were collected were supplied from a local store in Giza, Egypt. Most of the chemicals and reagents needed for the experiment were obtained from

Sigma Aldrich, including $Ti(NO_3)_4{\cdot}4H_2O$ (titanium(IV) nitrate tetrahydrate) as a titanium source, magnesium(II) nitrate hexahydrate ($Mg(NO_3)_2{\cdot}6H_2O$), $HAuCl_4{\cdot}3H_2O$ (hydrogen tetrachloroaurate(III) hydrate), and sodium hydroxide as a precipitating agent. MTT (3-(4,5-dimethyl-2-thiazolyl)-2,5-diphenyl-2*H*-tetrazolium-bromide), Taxol (paclitaxel), and DMSO (dimethyl sulfoxide) were purchased from Sigma Chemical Co. (Missouri, USA). Fetal bovine serum (FBS), phosphate buffer saline (PBS), trypsin-EDTA, and Dulbecco's modified Eagle's medium (DMEM), penicillin/streptomycin (Pen/Strep) were procured from Gibco (Gibco, TFS Inc., USA).

2.2 Banana peel extract preparation

Fresh bananas were sourced from local merchants, and their peels were sliced into small pieces and washed three times with distilled water to remove dirt and impurities. The cleaned peel pieces were dried using paper towels and boiled for 20 min at 100°C in a beaker containing 250 mL of double-distilled water and 100 g of peels. The resulting mixture was filtered three times using Whatman No. 1 filter paper, yielding a pale yellow extract, which was then refrigerated at 4°C for further use [32].

2.3 Biosynthesis of trimetallic TiO_2–MgO–Au NPs using banana peel extract

Ten milliliters of 0.01 M solutions of $Ti(NO_3)_4{\cdot}4H_2O$, $Mg(NO_3)_2{\cdot}6H_2O$, and $HAuCl_4{\cdot}3H_2O$ were precisely combined and stirred at room temperature for approximately 1 h. After that, the extracted banana peel (30 mL) was added following Kamli et al.'s [33] procedure with a few adjustments. Subsequently, 20 mL of the banana peel extract was added, adjusting the pH to 9.0. The optimal synthesis of trimetallic TiO_2–MgO–Au nanoparticles was achieved by maintaining the reaction conditions at an incubation temperature of 35°C with continuous agitation (250 rpm) in a shaking incubator for approximately 24 h [34]. At the end of the incubation period, the solution changed to a pale brown color, signifying the successful formation of trimetallic TiO_2–MgO–Au nanoparticles. To get rid of peel biomolecules that were weakly attached, the produced trimetallic TiO_2–MgO–Au NPs needed to be washed five times using distilled water. Afterward, the nanoparticles were separated by centrifugation at 15,000 rpm for 5 min, collected, and dried in an oven at 200°C overnight [35].

2.4 Characterization of trimetallic TiO_2–MgO–Au NPs

The color shift of the banana peel extract from pale yellow to pale brown upon mixing with the metal precursors is the first clue that the synthesis of trimetallic TiO_2–MgO–Au NPs has occurred. Then, UV-visible spectroscopy (JENWAY 6305, Staffordshire, UK) was used to determine the absorbance of the faint brown hue at wavelengths between 200 and 800 nm. The synthesized solution (2 mL) was put in a quartz cuvette, and its absorbance was determined at regular intervals at various wavelengths to find the maximum absorbance [36]. Moreover, the chemical functional groups included in the produced trimetallic TiO_2–MgO–Au NPs were determined by FTIR analysis (Cary-660 model, KBr pellet technique, wavenumber range: 400–4,000 cm^{-1}). Moreover, the surface morphology of trimetallic TiO_2–MgO–Au NPs was evaluated using SEM (ZEISS, EVO-MA10, Germany). Using EDX (Bruker, Germany), the elemental composition, purity, and distribution of the constituents in the produced trimetallic TiO_2–MgO–Au NPs were examined. Additionally, we used transmission electron microscopy (TEM) (JEM-2100 Plus, Jeol, Japan) to determine the morphologies, average, and exact sizes of the produced trimetallic TiO_2–MgO–Au NPs. The average particle size distribution and zeta potential analysis of the trimetallic TiO_2–MgO–Au NPs was determined using dynamic light scattering (DLS) (Nano ZS, Malvern, UK) [37]. The crystal size and crystallinity were evaluated by using XRD-6000 (Shimadzu Scientific Instruments, Japan).

2.5 Antibacterial activity

Green synthesized trimetallic TiO_2–MgO–Au NPs were tested against five different microbial strains: *B. subtilis* (ATCC 6633), *S. aureus* (ATCC 6538), *P. aeruginosa* (ATCC 9027), *E. coli* (ATCC 25922), and *Candida albicans* (ATCC 10231). Each microbial strain was evenly spread on sterile Petri plates containing Muller–Hinton agar using the agar diffusion well method, following incubation of pure strains grown in Muller–Hinton broth. Using a clean cork borer, four 7 mm circular wells were created in the plates. To assess antimicrobial efficacy, 0.1 mL of TiO_2 salt, MgO salt, $HAuCl_4$, and TiO_2–MgO–Au NPs were added to each well. The Petri dishes were then incubated at 37°C overnight, and the inhibition zones were measured [38,39].

2.6 Determination of MIC

Using the broth-based microdilution technique, the minimum inhibitory concentrations (MIC) of TiO_2–MgO–Au NPs were

found for *B. subtilis* (ATCC 6633), *S. aureus* (ATCC 6538), *P. aeruginosa* (ATCC 9027), *E. coli* (ATCC 25922), and *C. albicans* (ATCC 10231). TiO_2–MgO–Au NPs were already synthesized in various amounts (from 1,000 to 15.62 $\mu g \cdot mL^{-1}$). Different amounts of TiO_2–MgO–Au NPs were introduced to sterilized microtiter plate wells after 100 µL of double-strength Mueller–Hinton broth. Microbial cell suspension (20 µL) matching (OD of 0.5 McFarland standard) was added to all wells except the negative control well. Positive control wells were populated with microbial solutions to determine if MH broth would sustain microbial growth. These plates were incubated for 24 h at 37°C. The wells were then filled with 30 µL of HiMedia's resazurin solution (0.02% wt/v), and then the plate was incubated for a further 6 h to check for microbial growth. In cases when the strains had been propagated properly, the color of the developing control wells changed from blue to red, while the color of the control or negative control wells remained constant in the absence of contamination. Three runs of the examination were conducted [7].

2.7 Assay for biofilm inhibition

Using methicillin-resistant *S. aureus* (MRSA), clinically relevant isolation with a powerful biofilm-forming agent, the MTP technique was utilized to evaluate the ability of TiO_2–MgO–Au NPs to prevent or diminish the development of bacterial biofilms. We made some changes to the biofilm research to make it better than the previous one [5,40]. MTP-containing TSB media were added to gradient doses of TiO_2–MgO–Au NPs, supplemented with 1% glucose. The organisms investigated were cultivated on MH broth for 24 h at 37°C after being diluted 1:100 in TSB. The growth of the cell intensity (OD620 nm) was monitored during the incubation period, and then the planktonic cells were removed from the plates. The resultant biofilm was fixed for 10 min using 200 µL of 95% methanol as the solvent and washed three times using PBS at pH 7.4. This was done after removing all the components of the well contents so as not to disturb the biofilms that had grown. Once the 200 µL wells were filled with 0.3% w/v crystal violet, they were left at room temperature for around 15 min. Subsequently, the plates were washed using distilled water, and then the wells were filled with a 30% acetic acid reagent for the quantitative evaluation of biofilm formation. The absorbance was measured at OD 540 nm using the STATFAX-USA microplate reader. The results were confirmed by comparing the comparative wells that were treated with the untreated wells [7].

2.8 Anticancer activity

2.8.1 Cell viability assay

The study used two cell lines from ATCC (USA): HepG2, derived from hepatic cancer, and MCF-7, derived from breast cancer. The cells were cultured in DMEM supplemented with 10% FBS and 1% penicillin/streptomycin solution (TFS Inc., USA) at 37°C with 5% carbon dioxide. The MTT method was used to measure the cytotoxic capability [41]. The cells were distributed in 96-well plates with a mean density of 1.2×10^4 cells/well and incubated for 24 h to allow for development. Then, the medium containing different concentrations of nanoparticles was replenished. The MTT assay was performed after 48 h by introducing 100 µL of a solution comprising 5 $mg \cdot mL^{-1}$ MTT in PBS. The wells were then placed in an incubator set at body temperature for 4 h. DMSO (100 µL) was introduced to every well to form the crystals of formazan. The plates were incubated at body temperature for 10 min. Optical densities were measured at 570 nm and obtained using a microplate reader (Epoc-2 C, Bio Tek, USA).

2.8.2 Assessment of caspase-8 activity

ELISA kits from DRG International Inc. (USA) were used to determine caspase-8 activity (human, EIA-4863).

2.8.3 *In vitro* cell-based VEGFR-2 TK inhibitory assay

The inhibitory effect of TiO_2–MgO–Au NPs towards VEGFR-2 was assessed *in vitro* by applying ten-fold serial dilution procedures (1.0, 0.1, 0.01, 0.001 µM) employing the VEGFR-2 (KDR) Kinase Assay Kit (Catalog no. # 40325) following the manufacturer's instructions. Concisely, 25 µL per well of the mix was made and poured into every well. Inhibitor solution (5 µL) was added to every well, designated as a "Test Inhibitor." Then, 5 µL of an equal liquid without an inhibitor was added to the positive control and blank. Subsequently, 600 µL of kinase buffer and 2.4 mL of water were mixed to create a 3 mL kinase buffer. Twenty microliters of the kinase buffer were added to the "Blank" wells. The amount of VEGFR-2 required for the experiment was calculated, and kinase buffer was used to dilute the enzyme to a concentration of 1 $ng \cdot \mu L^{-1}$. Test Inhibitor Control and Positive Control wells were filled with 20 µL of diluted VEGFR-2 enzyme to initiate the reaction. The mixtures were incubated for 45 min in an incubator with a temperature setting of 30°C. Each well received a volume of 50 µL of

Kinase-Glo Max reagent. For 15 min, the plate was left at room temperature. Luminescence was measured using a microplate reader.

2.9 Statistical analysis

The GraphPad Prism 8.0 (CA, USA) was employed to conduct data assessment and graphical demonstrations. All findings are expressed as mean ± SD, and all investigations were done three times (n = 3). The statistical analysis was performed using a one-way analysis of variance and Tukey's multiple comparison tests, where $P < 0.05$ was considered significant.

3 Results and discussion

3.1 Biosynthesis of trimetallic TiO_2–MgO–Au NPs using banana peel extract

There are several advantages of using plant extracts for nanoparticle production as opposed to other biological synthesis methods that include microorganisms. Numerous aspects, including the minimal lab needs for nanoparticle synthesis, the appropriateness for commercial production, the avoidance of impurities, the speedier approach, the single-step process, handling safety, and the greater stability of the nanoparticles owing to significant metabolite secretion, all contribute to this conclusion [42]. The primary function of plant secondary metabolites, including phenols, carbohydrates, proteins, flavonoids, steroids, alkaloids, tannins, sugars, and terpenoids, is to reduce and stabilize nanoparticles [43]. Indeed, variability in biochemical composition poses challenges for reproducibility across batches; however, ensuring consistent processing conditions, such as using standardized ripeness levels or controlled extraction methods, is essential to mitigate these issues. In the present study, trimetallic TiO_2–MgO–Au NPs were prepared using an extract from banana peels. The high polyphenolic content in banana peel extract substantially enhances its reducing capacity, facilitating effective nanoparticle synthesis and improving its stability [44]. Banana peel extract contains functional groups such as carboxyl, amine, and hydroxyl groups, which act as reducing agents and stabilize nanoparticles by capping their surface [45]. Nanoparticle stability is influenced by several environmental factors, particularly pH and temperature. The stability of nanoparticles is highly sensitive to the pH of the medium in which they are stored. In highly acidic or alkaline environments, nanoparticles may undergo dissolution, aggregation, or surface modifications that affect their stability. For example, nanoparticles synthesized under more neutral conditions tend to exhibit better long-term stability. Under extreme pH conditions, the surface charge can change, leading to aggregation or destabilization. Studies have shown that nanoparticles with a neutral surface charge are more stable in a wide range of pH levels [46].

Temperature is another crucial factor influencing the long-term stability of nanoparticles. Higher temperatures can accelerate degradation processes such as oxidation, agglomeration, or changes in surface charge. The stability of nanoparticles is generally improved when they are stored at lower temperatures, as this slows down the rate of degradation reactions. However, long-term storage at high temperatures may lead to the transformation or sintering of nanoparticles, potentially resulting in a decrease in their functional properties. For instance, nanoparticles that are stored at room temperature or under refrigeration often exhibit greater stability and retain their biological activity for extended periods [47]. Trimetallic nanostructures, which are subsequently stabilized and capped, are produced as a result of metabolites in the banana peel extract decreasing the metal precursors. A simple and eco-friendly process was developed by Dlugaszewska and Dobrucka [48] to generate Au/Pt/Ag trimetallic nanoparticles using an aqueous *Lamii albi* flos extract. Furthermore, *Meliloti officinalis* extract was used to bio-prepare Au–ZnO–Ag trimetallic nanoparticles (~20 nm) [49]. Aqueous leaf extracts of *Froriepia subpinnata* and *Eryngium campestre* were used to biosynthesize Cu/Cr/Ni trimetallic oxide nanoparticles reliably at moderate temperatures [50]. These NPs demonstrated exceptional antibacterial activities against *E. coli* and *S. aureus*. Rao and Paria [51], by modifying the mix of phytochemicals in extracts from *Aegle marmelos* (leaf extract) and *Syzygium aromaticum* buds, alloy-like Ag–Au–Pd trimetallic NPs (~8–11 nm) were green-fabricated in 10 min under ambient conditions. In another study, Kaur et al. [52] synthesized TiO_2–Al_2O_3–$ZnFe_2O_4$ nanocomposites using hydrothermally prepared *Hibiscus rosa* sinesis flower extract. Furthermore, *Aspergillus niger* was successfully used in the entire mycosynthesis of trimetallic copper, selenium, and zinc oxide nanoparticles (Tri-CSZ NPs) by Hashem et al. [27].

3.2 Characterization

3.2.1 UV–vis spectroscopy

The first indication of trimetallic TiO_2–MgO–Au NPs production is the plant's aqueous extract changing from pale

yellow to pale brown after being mixed with $Ti(NO_3)_4{\cdot}4H_2O$, $Mg(NO_3)_2{\cdot}6H_2O$, and $HAuCl_4{\cdot}3H_2O$. This change validated the ability of metabolites to reduce metal ions and build nanoscale structures. The new hue's absorbance was measured between 200 and 800 nm to determine the maximum SPR. There were two maximums of SPR at 270 and 550 nm, which corresponded to (TiO_2, MgO) and Au absorbance, respectively (Figure 1). An absorption band associated with phytobiomolecules may be seen at 280 nm in the UV-visible spectra of banana peel extract. Hassan et al. [53] verified the excitation of green-synthesized TiO_2 NPs using a UV–Vis spectrophotometer at 270 and 290 nm. Furthermore, the specific absorption peak was observed at 267 nm for magnesium oxide nanoparticles synthesized by using *Trigonella foenum-graecum* leaf extract by Vergheese and Vishal [54]. According to Hassanisaadi et al. [55], the UV-Vis spectra of biosynthesized AuNPs were observed at 545 nm.

According to many studies conducted by Alshehri and Malik, the biosynthesis of trimetallic Cu–Co–Ni NPs utilizing an extract of *Origanum vulgar* L. shows absorption peaks in its UV–visible spectra at 270 and 320 nm [34]. The green-produced NPs from the combined leaf extracts of *F. subpinnata* and *E. campestre* had the highest absorbance at about 220 nm, according to Vaseghi et al. [50]. It is crucial to keep in mind that the interaction of numerous chemicals in the reaction mixture may prevent separate peaks from forming for each of the individual metals that make up the trimetallic structure. As shown by Kannaiyan et al. [56], the UV–Vis absorbance of the *C. sativum* extract was compared with the collected tri-metallic oxide NPs. The three distinctive peaks of tri-metallic oxide NPs, which exhibited wavelengths of 261 nm, 426 nm, and 564 nm, correspond to the tri-metallic oxide Ni/Cr/Cu NPs, as previously reported. Furthermore, Vaseghi et al. [50] observed that the nanocomposite's absorption spectra showed the appearance of the largest absorption peak at 265 nm, which suggested the existence of a distinct surface plasmon resonance.

3.2.2 FT-IR spectroscopy

FT-IR spectroscopy was used to identify the trimetallic TiO_2–MgO–Au NPs that were biosynthesized. The FT-IR spectra of the synthetic composite are in the 400–4,000 cm^{-1} spectral region. Ten distinct peaks at wavenumbers 3,200, 2,668, 2,340, 2,076, 1,830, 1,643, 1,405, 1,095, 570, and 439 cm^{-1} were found in the FT-IR spectra of trimetallic TiO_2–MgO–Au NPs (Figure 2). Several groups found in banana peel extract belonged to a variety of substances, including proteins, amino acids, amines, and polysaccharides. The peaks at 3,200, 2,668, 2,340, 2,076, 1,830, and 1,095 cm^{-1} are caused by the stretching bonds of O–H, C–H, C═O, C═C, and C–O, respectively, that are found in bioorganic molecules such as phenolics, amino acids, and carboxylic acid compounds [57]. Conversely, the nanocomposite's spectrum displayed all of these vibrations at a greater intensity because of the weak van der Waals contacts between the metallic and biological NPs [58]. According to Botteon et al. [59], metal–metal interactions inside the nanocomposite are responsible for the new, strong bands in the 400–600 cm^{-1} range. Both the new bands at 1,643 and 1,405 cm^{-1}, which are often associated with the stretching and bending vibrations of the carboxylate anion [60], most likely resulted from the oxidation of –C–OH

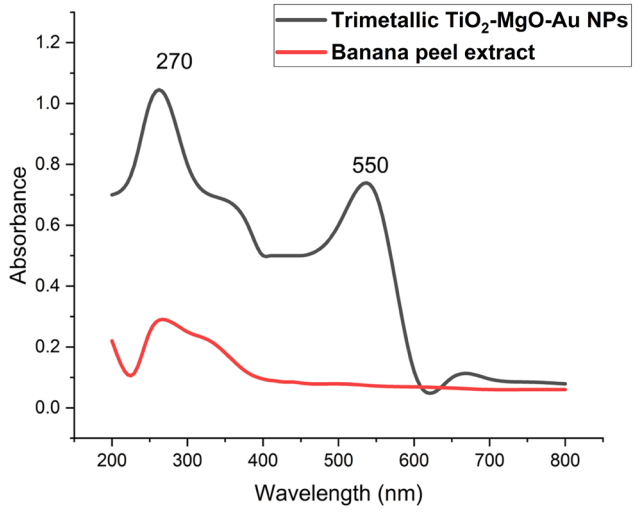

Figure 1: UV-Vis spectroscopy of banana peel extract and biosynthesized trimetallic TiO_2–MgO–Au NPs.

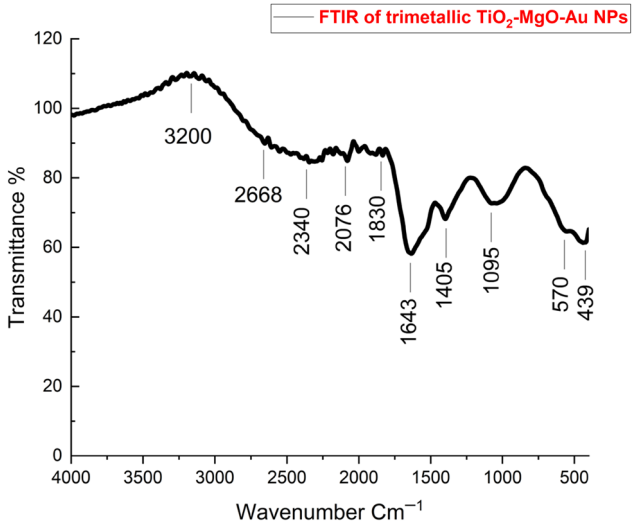

Figure 2: FTIR analysis of biosynthesized trimetallic TiO_2–MgO–Au NPs using banana peel extract.

in phytochemicals during the reduction of metal ions [61]. The results are consistent with previous studies [34,50,57] on the manufacture of trimetallic nanoparticles using plant aqueous extract.

3.3 Morphological and elemental analysis

TEM and SEM were used to examine the surface morphology and particle size of the biosynthesized TiO_2–MgO–Au NPs (Figure 3). In this case, an extract from banana peels was used to create trimetallic TiO_2–MgO–Au NPs; while many plant extracts share similar properties, the composition of banana peel extract, especially its polysaccharides and high antioxidant levels, offers distinct benefits in creating smaller, more uniform nanoparticles with robust stability [62]. TEM was used to examine their distribution, size, and shape. The produced trimetallic TiO_2–MgO–Au NPs, in this instance, had spherical forms and ranged in size from 50 to 70 nm, with an average size of 55 nm (Figure 3a). Therefore, smaller nanoparticles are more reactive in biological environments [63]. Similarly, Hussein et al. [57] claim that TEM images display the spherical form of nanoparticles with a particle size of 50–90 nm. Vaseghi et al. [50] revealed that the TEM images of Cu/Cr/Ni trimetallic oxide NPs biosynthesized by aqueous leaf extracts of *E. campestre* and *F. subpinnata* show a variety of sizes and shapes.

The nanocomposite's morphology was examined using SEM. Figure 3b displays the recorded SEM images. Because of the high surface energy-imposed strong interparticle contact, the trimetallic composite structure displayed an oval and irregular crystalline porous structure, which is characteristic of metallic nanocomposites. When smaller nanostructures merge to form larger ones, the result is a mixed nanostructure. This is evident in the SEM images and indicates the formation of a nanocomposite [57]. Additional research by Alshehri and Malik [34] demonstrates through SEM micrographs of biosynthesized Cu–Co–Ni

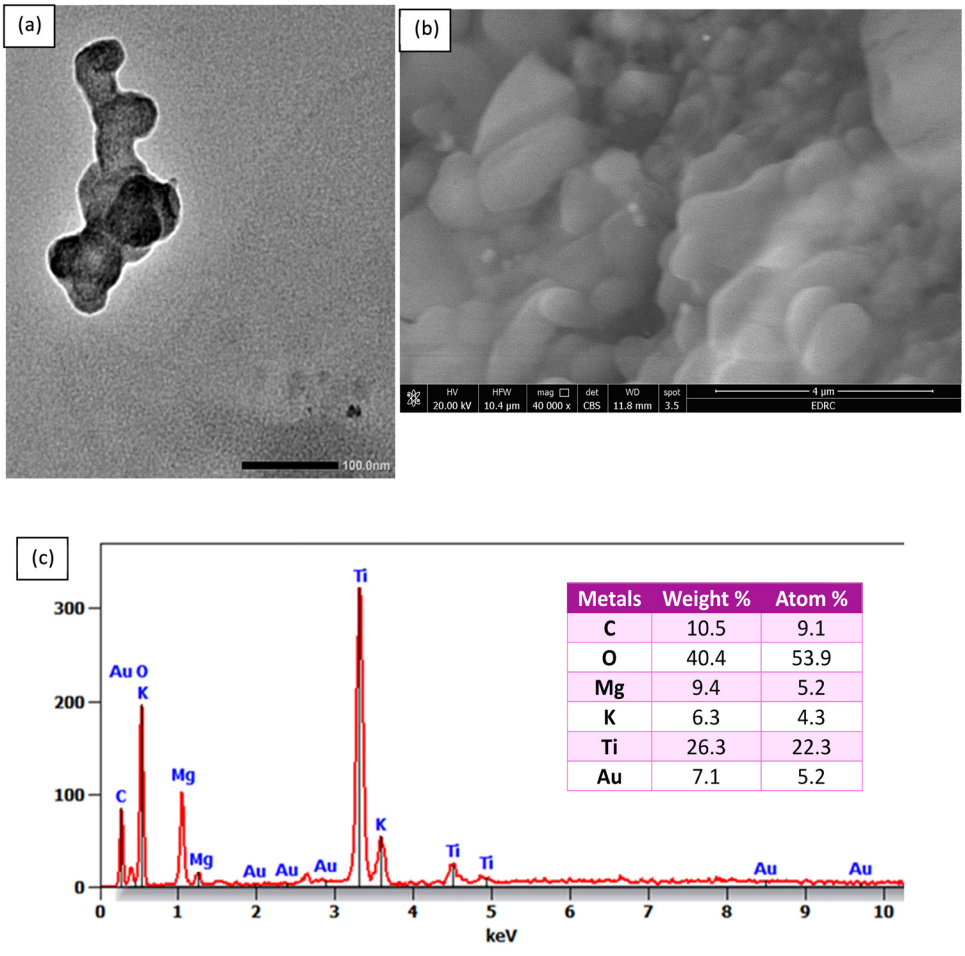

Figure 3: (a) TEM image, (b) SEM image, and (c) EDX analysis of biosynthesized trimetallic TiO_2–MgO–Au NPs by using banana peel extract.

trimetallic nanoparticles that structural porosity is caused by the agglomeration of nanoflakes.

Verifying the presence and distribution of the required metals inside the trimetallic structure can be facilitated by EDX analysis, which offers information on the elemental composition of a nanostructure. Knowing the elemental composition of NPs is essential to creating materials with appropriate qualities and their use for certain applications. Using EDX analysis, the trimetallic TiO_2–MgO–Au NPs' elementary mapping was determined. According to the acquired data, the as-formed sample mostly consists of Ti, Mg, O, and Au ions, as shown by their respective weight percentages (26.3%, 9.4%, 40.4%, and 7.1%) and atomic percentages (22.3%, 5.2%, 53.9%, and 5.2%) (Figure 3c). The trimetallic synthesis that was previously studied using chemical techniques and plant or microbial extracts was consistent with our findings [34,50]. Plant extract capping agents that coat nanoparticles for stability may be the cause for the C and K peaks [64]. Alshehri and Malik [34], using EDX analysis, determined the weight percentages of 17.34% Co, 10.37% Ni, and 34.01% Cu, resulting in a 2:1:3 ratio for the Cu–Co–Ni trimetallic nanoparticles made with the extract from *Origanum vulgare* L. in a different study. It appears that surface biomolecules act as capping agents when weak C and O signals are present, and in the elemental mapping, Ni is shown in white, Co in green, and Cu in red.

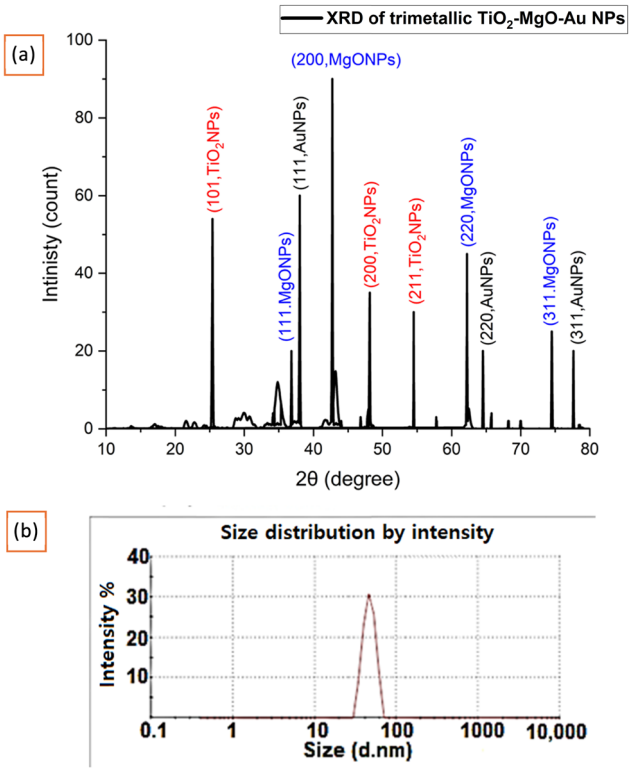

Figure 4: XRD (a) and DLS (b) of the biosynthesized trimetallic TiO_2–MgO–Au NPs.

3.4 XRD, DLS, and zeta potential analysis

The trimetallic TiO_2–MgO–Au NPs were examined using XRD. The trimetallic TiO_2–MgO–Au NPs XRD spectra, as displayed, revealed ten powerful reflection peaks at 2θ of 25.4°, 36.8°, 38.0°, 42,7°, 48.1°, 54.5°, 62.2°, 64.5°, 74.5°, and 77.6°, respectively. These represent the Bragg diffraction of the (101), (111), (200), (211), (220), and (311) planes, as shown in Figure 4a. Upon analyzing the produced nanoparticles using XRD, they found unique diffraction peaks at four different angles: 25.4°, 38.0°, 48.1°, and 54.5°. These angles correspond to the (101), (111), (200), and (211) planes, respectively, and are in line with a typical TiO_2-NP phase pattern (JCPDS No. 21-1272) [65]. MgO-NPs exhibited characteristic peaks at 2θ values of 36.8°, 42,7°, 62.2°, and 74.5°, corresponding to the (111), (200), (220), and (311) planes (JCPDS: 9000493) [66]. Five distinct diffraction peaks were discovered for the hexagonal structure of Au-NP, and they were indexed with the planes (111), (220), and (311) at 38.0°, 64.5°, and 77.6°, respectively (JCPDS: 00-407-84) [67]. These peaks lined up with certain crystallographic planes, such as (220), (211), (211), (111), (200), and (311). Notably, the crystalline structure of the trimetallic TiO_2–MgO–Au NPs was verified by these peaks. Using Scherrer's equation and the XRD pattern, the average crystallite size of the trimetallic TiO_2–MgO–Au NPs was found to be 60 nm. The discrepancy between DLS and TEM's recorded size values of vesicles is expected. This is because the sample preparation for TEM measurement involves dehydration and staining, which can affect the size. Moreover, DLS provides an average size for particles moving in dispersion and is highly sensitive to particle agglomeration or clustering. Even minor aggregation can significantly increase the measured hydrodynamic diameter, as DLS calculates an average size weighted by the intensity of scattered light, but TEM captures a specific field. A similar discrepancy was noticed in previous work and was discussed similarly [68]. The trimetallic nanocomposite (Ru/Ag/Pd) XRD patterns were shown by Hussein et al. [57], and the (111), (200), and (220) planes of Pd-NP were matched with the high-intensity peaks at 2θ = 40.11, 47.75, and 68.31, which match JCPDS 87-0641. At 2θ values of 38.45°, 44.85°, 67.55°, and 77.5°, Ag-NPs showed peaks that corresponded to the (111), (200), (220), and (311) planes, respectively (JCPDS: 04-0783). Ru-NPs revealed peaks for the (100), (002), (101), (102) planes (69.42°, 43.82°, 46.12°, 58.32°, and 69.42°) (JCPDS: 06–0663). Pure crystalline trimetallic nanoparticles were present since no

impurity peaks were seen. By using Scherrer's equation, the crystal size was determined to be 15.67 nm. The same result was obtained by Alshehri and Malik [34] for biogenic Cu–Co–Ni trimetallic nanoparticles.

The size distribution of the particles in a suspension or solution may be measured using the DLS method. It offers details on how different particle sizes are distributed within a sample; this information is commonly shown as a histogram or intensity-weighted size distribution curve. Particle populations that are polydisperse (varying in size) or monodisperse (uniform in size) can be identified by the analysis. DLS examination of the trimetallic TiO_2–MgO–Au NPs revealed an average particle size distribution of about 70 nm (Figure 4b). They came to the conclusion that the greater size might have been caused by trace quantities of larger particles formed by contamination or agglomeration, which could add uncertainty to particle size measurements [69]. Similarly, the particle size was roughly 190 nm for the Cu–Fe–Ag NPs that were subjected to DLS analysis by Roy et al. [70]. Monodisperse models are more consistent with the polydispersity index (PDI) values of less than 0.05. Conversely, values higher than 0.7 are expected to indicate the dispersion of polydispersity particles [71]. In this study, the PDI value was 0.472 for the approved PDI levels. The present data show that the trimetallic TiO_2–MgO–Au NPs biosynthesized have a moderately polydisperse size distribution.

The zeta potential is a key parameter in assessing the colloidal stability of nanoparticle suspensions, influenced by factors such as surface chemistry, particle roughness, and adsorbed biomolecules [101]. A high absolute zeta potential value (greater than ±30 mV) typically indicates strong electrostatic repulsion, preventing aggregation and ensuring stability [102]. Conversely, values approaching 0 mV suggest reduced repulsive forces, leading to particle agglomeration. Some studies suggest that particles with zeta potential values exceeding ±20 mV can still exhibit moderate stability, depending on other stabilizing interactions [103,104].

In this study, the biosynthesized trimetallic TiO_2–MgO–Au NPs exhibited a bimodal zeta potential distribution, with peaks at approximately −20 and +25 mV, indicating a heterogeneous surface charge, as shown in Figure 5. This variation may result from differences in the particle size, surface composition, or functional groups adsorbed from the biological extract used in the synthesis [102]. In this study, the observed zeta potential values indicate a moderate level of colloidal stability, which aligns with the PDI value (0.472), confirming the polydisperse nature of the synthesized nanoparticles. El-Sawaf et al. [105] reported a zeta potential of 21.5 mV for the trimetallic CuO/Ag/ZnO nanocomposite synthesized using *Ziziphus spina-christi* plant extract.

3.5 Antimicrobial activity of trimetallic TiO_2–MgO–Au NPs

In the present investigation, the agar well-diffusion technique was used to evaluate the antimicrobial performance of biologically generated TiO_2–MgO–Au NPs against a variety of five microbial pathogens, including Gram-positive (*S. aureus* ATCC 6538, *B. subtilis* ATCC 6633), Gram-negative (*E. coli* ATCC 25922, *P. aeruginosa* ATCC 9027), and *C. albicans* ATCC 10231. TiO_2–MgO–Au NPs strongly inhibited *C. albicans, S. aureus, B. subtilis, E. coli*, and *P. aeruginosa* by 33.8 ± 0.25 mm, 36.6 ± 0.75 mm, 24.7 ± 0.55 mm, 23.16 ± 0.4 mm, and 25.9 ± 0.32 mm, respectively, when compared to each microbe's area of inhibition (Figure 6).

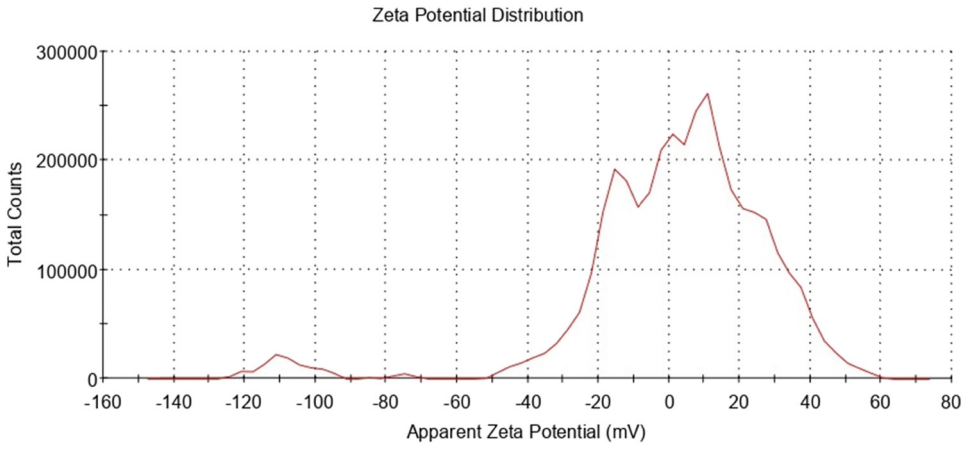

Figure 5: Zeta potential analysis of the biosynthesized trimetallic TiO_2–MgO–Au NPs.

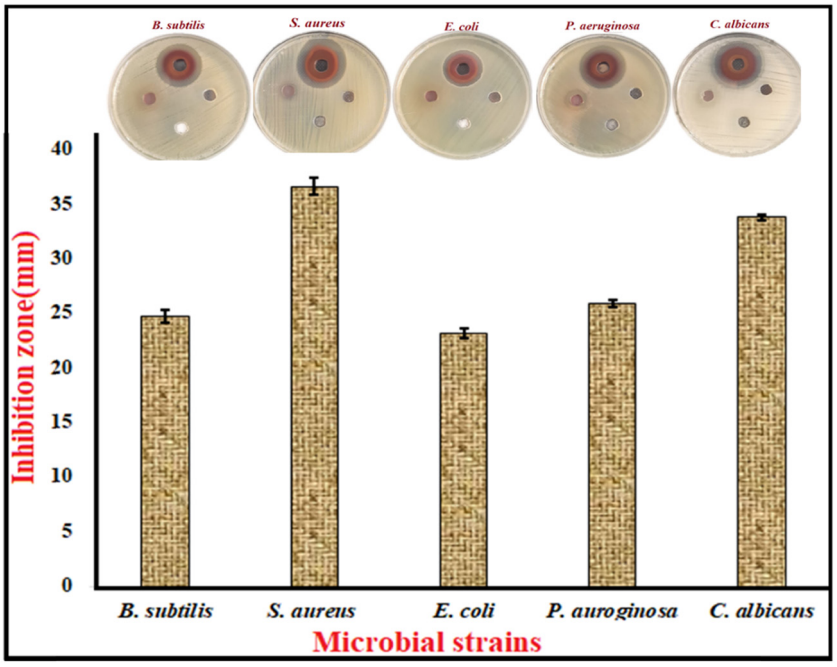

Figure 6: Antimicrobial activity of trimetallic TiO_2–MgO–Au NPs using the agar well technique.

The inhibitory impact of various concentrations of TiO_2–MgO–Au NPs (15.62–1,000 μg·mL^{-1}) was examined to determine the MICs of the NPs against the indicated microbial pathogens. The lowest MIC for *S. aureus* was 125 μg·mL^{-1}, whereas the MIC for *P. aeruginosa* and *C. albicans* was 250 μg·mL^{-1}, and that for *B. subtilis* and *E. coli* was 500 μg·mL^{-1} (Figure 7). The obtained result was consistent with studies concerning the antibacterial efficacy of trimetallic nanoalloys [72,73]. Multiple studies indicated that the efficacy of nanoparticles versus diverse pathogenic bacteria was ranked (from highest to lowest) as follows: tri, bi, and monometallic. The trimetallic Au/Pt/Ag exhibited superior antibacterial efficacy *against E. faecalis, S. aureus, E. coli*, and *C. albicans* in comparison to monometallic variants [48]. One possible explanation for this action is the additive nature of trimetallic compounds as opposed to bi- or monometallic ones [74].

The FDA has also approved MgO NPs for use as harmless substances [75]; they received research attention for their potential use in biological fields. Magnesium oxide

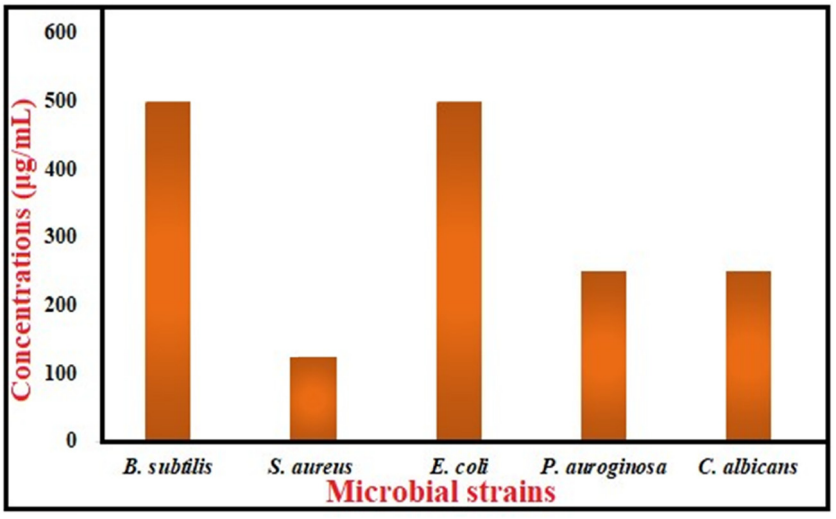

Figure 7: MIC of trimetallic TiO_2–MgO–Au NPs toward the tested microbial strains.

nanoparticles (MgO NPs) are non-toxic and easily obtainable and have antibacterial characteristics against both Gram-positive and Gram-negative bacteria, fungi, and viruses, along with traits that limit biofilm formation [76,77]. MgO NPs have shown their ability to inhibit *S. aureus, P. aeruginosa*, along with *E. coli* [75,78]. They prevented *K. pneumoniae* and *S. aureus* from forming biofilms [77]. TiO_2 NPs were demonstrated to have antimicrobial capabilities against a variety of bacteria, including *E. coli, S. aureus, P. aeruginosa*, and *P. expansum* [79]. Enhanced antimicrobial effectiveness of AuNPs towards Gram-negative bacteria has been found; this may be because of thinner cell walls and more sustained electrostatic contacts [80]. It has been noted that the type of microbe and strain, as well as the size, functionalization, and quantity of AuNPs, directly affect the antibacterial action [81]. Here, NPs serve as antimicrobial substances that can be employed to administer traditional antimicrobials or to fight resistance to antimicrobial treatments directly. The potential of NPs to enter and damage microbial cell membranes through membrane-damaging hardness, reduce cellular permeability, or generate antimicrobial properties (e.g., the generation of ROS, interactions between proteins and nucleic acids, deactivation of enzymes, excessive expression regarding efflux pumps and expulsion of metal ions), and prevent the development of biofilms [82–84]. The trimetallic (TiO_2–MgO–Au) NPs can inhibit pathogenic microbes via impact on the cell wall, cell membrane, and protein synthesis that leads to suppressing the activity of the microbes as mentioned in previous studies [28,85,86].

3.6 Anti-biofilm activity of trimetallic TiO_2–MgO–Au NPs

The antibiofilm efficacy of TiO_2–Mg–ZnO) NPs against *S. aureus* MRSA in the current investigation showed significant results. Thus, when used at quantities below the MIC amount, TiO_2–MgO–Au NPs displayed the greatest efficacy against the development of biofilms caused by MRSA: 250, 125, 62.5, 31.25, and 15.62 $\mu g \cdot mL^{-1}$ decreased the generation of biofilm by 86.8%, 77.1%, 63.3%, 53.4%, 37.6%, and 25.1%, respectively. (Figure 8). According to their respective quantitative and qualitative assessments, TiO_2–MgO–Au NPs prevented the very initial stages of MRSA biofilm creation. The biofilm inhibition results using crystal violet were in agreement with those of Khan et al. [87].

It was found that *P. aeruginosa* biofilms were inhibited by intracellularly produced gold nanoparticles employing *Laccaria fraternal*. The nanoparticles' gold content was about 15%, and they had a 93% reduction in biofilms [88]. AuNPs showed notable biofilm inhibition against *P. aeruginosa* and *E. coli* with sub-MICs, according to Anwar et al. [89]. At concentrations that ranged from 0.25 to 0.5× MICs, the nanocomposite, including AuNPs along with reduced graphene oxide (Au-RGO), showed comparable results, dependent on concentration, removal of established mature biofilms of MRSA and *P. aeruginosa* [90]. Moreover, the MIC of TiO_2 NPs demonstrated strong antibiofilm action towards *P. aeruginosa* by successfully obstructing the planktonic cells' adhesion to the substratum [91]. According to Achudhan et al., G-TiO_2 NPs were evaluated against fungus (*C. albicans*) as well as bacteria (*Citrobacter freundii* and *S. mutans*) to determine

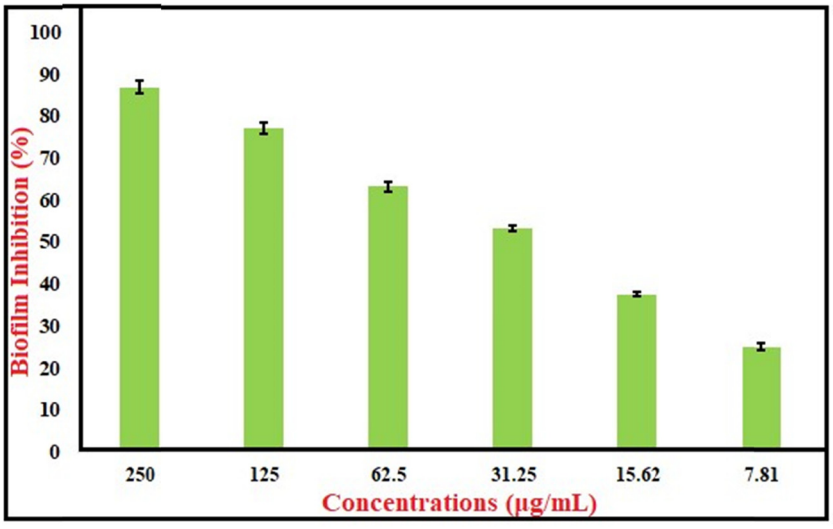

Figure 8: Antibiofilm activity of trimetallic TiO_2–MgO–Au NPs.

their antimicrobial and antibiofilm properties. At 100 μg·mL^{-1}, each of the fungus and bacterial biofilms were significantly suppressed [92]. Mg-NPs inhibited the biofilms of *S. pyogenes, S. epidermis,* and *P. aeruginosa* by 87.15%, 76.35%, and 49.14%, respectively, at an average concentration of 0.98 μg·mL^{-1}. The bacteria in concern had the same minimal biofilm inhibitory concentrations (MBICs) of 1.95 μg·mL^{-1} for the first two strains and 7.81 μg·mL^{-1} for *P. aeruginosa* [93]. The effectiveness of TMNC in inhibiting biofilm generation by *S. aureus* as well as *E. coli* was assessed by employing crystal violet staining, as noted in prior research, at different inhibition percentages. Elevated TMNC doses inhibited biofilm creation by *S. aureus* and *E. coli* by 85% and 83%, respectively [94]. The biofilm inhibition proportion of the nanocomposite for both bacterial strains increased with a higher TMNC ratio. This is due to the antibiofilm capability of TMNCs. The quantity of TMNC enhances biofilm inhibition and also increases for both bacterial strains. This followed a prior publication by Garza-Cervantes et al. about the progressive reduction in biofilm development as the amount of composite nanoparticles increased [95].

3.7 Cytotoxic effect of TiO_2–MgO–Au NPs

The cytotoxic activities of TiO_2–MgO–Au NPs were assessed on HepG2 and MCF-7. The MCF-7 cells exhibited the most significant cytotoxic impact, as evidenced by their minimal IC_{50} values (Figure 9). TiO_2–MgO–Au NPs resulted in a minimal IC_{50} value of 11.09 ± 1.02 μg·mL^{-1}, while the IC_{50} for taxol was 8.96 ± 0.98 μg·mL^{-1}. The MCF-7 cells are more susceptible to the cytotoxic effects of TiO_2–MgO–Au NPs due to their increased expression of receptors and cell surface markers in breast cancer cells, which increase susceptibility. Conversely, HepG2 cells exhibit a greater antioxidant capacity than MCF-7 cells. This antioxidant defense can potentially reduce the cytotoxic activity of TiO_2–MgO–Au nanoparticles toward HepG2 cells, thereby mitigating their cytotoxic effects [96,97].

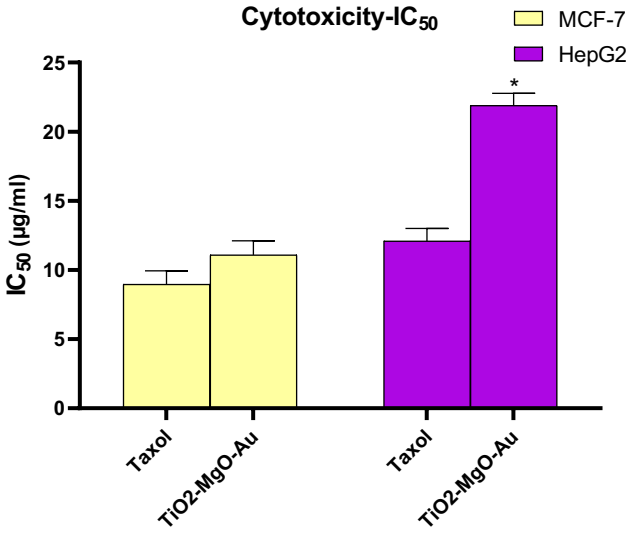

Figure 9: *In vitro* cytotoxic effects of TiO_2–MgO–Au towards MCF-7 and HepG2 cell lines. The data are displayed as the mean ± SD obtained from three separate and independent trials. *Statistically significant within the Taxol group at $p < 0.001$.

Table 1: Effect of TiO_2–MgO–Au on caspase-8 (ng·mL^{-1}) in MCF-7 cells in comparison to taxol; data are displayed as mean ± SD

Comp. ID	Caspase-8 (ng·mL^{-1}) MCF-7
Control	0.341 ± 0.02
Taxol	0.986 ± 0.03
TiO_2–MgO–Au	1.095 ± 0.04

3.8 Effect of TiO_2–MgO–Au NPs on caspase-8 activity

TiO_2–MgO–Au NPs influence the apoptotic marker caspase-8 (Table 1). Exposure of MCF-7 cells to TiO_2–MgO–Au NPs significantly increased caspase-8 activity (1.095 ± 0.04 ng·mL^{-1}) in comparison to the control (0.341 ± 0.02 ng·mL^{-1}). Furthermore, when exposed to TiO_2–MgO–Au NPs, caspase-8 activity was significantly higher compared with Taxol treatments (0.986 ± 0.03 ng·mL^{-1}). Apoptosis triggers the activation of DNA fragmentation enzymes by activating caspase-8 [98]. These compounds induced apoptosis in MCF-7 cells by activating caspase-8.

3.9 Effect of TiO_2–MgO–Au NPs on VEGFR-2 activity

Using the inhibition concentration–response curve, the 50% inhibition concentration value (IC_{50}) was found. The

Table 2: Effect of TiO_2–MgO–Au on VEGFR-2 in MCF-7 cells compared to Sorafenib

Comp. ID	VEGFR-2 IC_{50} (μg·mL^{-1}) MCF-7
Sorafenib	0.141 ± 0.005
TiO_2–MgO–Au	0.305 ± 0.018*

*Statistically significant from the sorafenib group at $p < 0.001$.

positive control used in this experiment was sorafenib. The comparison of IC_{50} values for VEGFR-2 inhibition between TiO_2–MgO–Au and the established inhibitors like sorafenib reveals significant differences in their potential anti-angiogenic activities. The close IC_{50} values of TiO_2–MgO–Au to sorafenib suggest that these differences may not be substantial. An IC_{50} value of 0.305 ± 0.018 $\mu g \cdot mL^{-1}$ for the TiO_2–MgO–Au NPs indicated a strong inhibitory effect (Table 2).

Breast cancer cells exhibit elevated VEGF expression in comparison to normal tissues. The anti-angiogenic effect is suggested by the decreased expression of the VEGF receptor (VEGFR-2). VEGF is a powerful angiogenic agent that stimulates the formation of blood vessels, angiogenesis, and the development of tumors in breast cancer. However, a reduction in VEGFR-2 expression hampers the capacity of VEGF to promote angiogenesis. The simultaneous decrease in VEGFR expression might result in a decline in the formation of new blood vessels, which can be advantageous in cancer therapy, where excessive blood vessel formation can promote tumor development and spread [99,100].

4 Conclusion

The current study successfully demonstrated the green biosynthesis of novel trimetallic TiO_2–MgO–Au NPs using banana peel extract for the first time. Detailed characterization revealed that the TiO_2–MgO–Au NPs were spherical with an average size of 55 nm. The biosynthesized TiO_2–MgO–Au NPs exhibited potent antimicrobial and antibiofilm activities, with the lowest MIC of 125 $\mu g \cdot mL^{-1}$ against *S. aureus*. Moreover, the TiO_2–MgO–Au NPs demonstrated significant cytotoxic effects on breast cancer cells (MCF-7), with an IC_{50} value of 11.09 ± 1.02 $\mu g \cdot mL^{-1}$, which was achieved through the activation of caspase-8 and the minimization of VEGFR-2 levels. These findings highlight the promising potential of the green-synthesized trimetallic TiO_2–MgO–Au NPs as a multifunctional nanomaterial with antimicrobial, antibiofilm, and anticancer properties, which can have valuable applications in the biomedical field.

Acknowledgments: The authors extend their appreciation to the ongoing Research Funding Program (ORF-2025-552) King Saud University, Riyadh, Saud Arabia.

Funding information: The authors extend their appreciation to the ongoing Research Funding Program (ORF-2025-552) King Saud University, Riyadh, Saud Arabia.

Author contributions: Mohamed Khalil Yousef Soliman: formal analysis, investigation, methodology, resources, software; and writing – original draft; Ahmed Soliman Doghish: conceptualization, investigation, project administration, supervision, visualization, and validation; Amr Hosny Hashem: conceptualization, data curing, formal analysis, investigation, methodology, project administration, resources, software, validation, visualization, writing-original draft, and writing – review and editing; Mostafa Abdel-Maksoud: data curing, formal analysis, and investigation; Walaa Ahmed El-Dakroury: conceptualization, data curing, formal analysis, investigation, and methodology; Abdulaziz Alamri: software, validation, and visualization; hossam ebaid: formal analysis, investigation, and methodology; Mohamed Sayed Hasanin: investigation, methodology, resources, and software; Ebrahim Saied: conceptualization, data curing, formal analysis, investigation, methodology, project administration, resources, software, validation, visualization, writing-original draft, and writing – review and editing.

Conflict of interest: Authors state no conflict of interest.

Data availability statement: The datasets generated during and/or analyzed during the current study are available from the corresponding author on reasonable request.

References

[1] Vimbela GV, Ngo SM, Fraze C, Yang L, Stout DA. Antibacterial properties and toxicity from metallic nanomaterials. Int J Nanomed. 2017;24:3941–65. doi: 10.2147/IJN.S134526. PMID: 28579779.

[2] Roy R, Tiwari M, Donelli G, Tiwari V. Strategies for combating bacterial biofilms: A focus on anti-biofilm agents and their mechanisms of action. Virulence. 2018;9(1):522–54. doi: 10.1080/21505594.2017.1313372. PMID: 28362216.

[3] Ibrahim SA, Fayed EA, Rizk HF, Desouky SE, Ragab A. Hydrazonoyl bromide precursors as DHFR inhibitors for the synthesis of bis-thiazolyl pyrazole derivatives; antimicrobial activities, antibiofilm, and drug combination studies against MRSA. Bioorg Chem. 2021;116:105339. doi: 10.1016/j.bioorg.2021.105339. PMID: 34530234.

[4] Nassar O, Desouky SE, El-Sherbiny GM, Abu-Elghait M. Correlation between phenotypic virulence traits and antibiotic resistance in Pseudomonas aeruginosa clinical isolates. Microb Pathogenesis. 2022;162:105339. doi: 10.1016/j.micpath.2021.105339. PMID: 34861345.

[5] Soliman MK, Salem SS, Abu-Elghait M, Azab MS. Biosynthesis of silver and gold nanoparticles and their efficacy towards antibacterial, antibiofilm, cytotoxicity, and antioxidant activities. Appl Biochem Biotechnol. 2023;195(2):1158–83. doi: 10.1007/s12010-022-04199-7. PMID: 36342621.

[6] Waters EM, Rowe SE, O'Gara JP, Conlon BP. Convergence of Staphylococcus aureus persister and biofilm research: can biofilms be defined as communities of adherent persister cells? PLoS Pathog. 2016;12(12):e1006012. doi: 10.1371/journal.ppat.1006012. PMID: 28033390.

[7] Soliman MK, Abu-Elghait M, Salem SS, Azab MS. Multifunctional properties of silver and gold nanoparticles synthesis by Fusarium pseudonygamai. Biomass Convers Biorefin. 2024;14(22):28253–70.

[8] Huh AJ, Kwon YJ. "Nanoantibiotics": a new paradigm for treating infectious diseases using nanomaterials in the antibiotics resistant era. J Control Release. 2011;156(2):128–45. doi: 10.1016/j.jconrel.2011.07.002. PMID: 21763369.

[9] Brianna, Lee SH. Chemotherapy: how to reduce its adverse effects while maintaining the potency? Med Oncol. 2023;40(3):88. doi: 10.1007/s12032-023-01954-6. PMID: 36735206.

[10] Shehabeldine AM, Doghish AS, El-Dakroury WA, Hassanin MM, Al-Askar AA, AbdElgawad H, et al. Antimicrobial, antibiofilm, and anticancer activities of syzygium aromaticum essential oil nanoemulsion. Molecules. 2023;28(15):5812. doi: 10.3390/molecules28155812. PMID: 37570781.

[11] El-Sayyad GS, Elfadil D, Mosleh MA, Hasanien YA, Mostafa A, Abdelkader RS, et al. Eco-friendly strategies for biological synthesis of green nanoparticles with promising applications. BioNanoScience. 2024;2:1–43.

[12] Wang C, Zhang S. Advantages of nanomedicine in cancer therapy: A review. ACS Appl Nano Mater. 2023;6(24):22594–610.

[13] Saied E, Abdel-Maksoud MA, Alfuraydi AA, Kiani BH, Bassyouni M, Al-Qabandi OA, et al. Endophytic Aspergillus hiratsukae mediated biosynthesis of silver nanoparticles and their antimicrobial and photocatalytic activities. Front Microbiol. 2024;15:1345423. doi: 10.3389/fmicb.2024.1345423. PMID: 38533339.

[14] Annu, Bhat ZI, Imtiyaz K, Rizvi MM, Ikram S, Shin DK. Comparative study of ZnO-and-TiO_2-nanoparticles-functionalized polyvinyl alcohol/chitosan bionanocomposites for multifunctional biomedical applications. Polymers. 2023;15(16):3477. doi: 10.3390/polym15163477. PMID: 37631534.

[15] Tas A, Cakmak NK, Agbektas T, Silig Y. Cytotoxic activity of zinc oxide/titanium dioxide nanoparticles on prostate cancer cells. Int J Chem Technol. 2019;3(2):113–20.

[16] Saied E, Hashem AH, Ali OM, Selim S, Almuhayawi MS, Elbahnasawy MA. Photocatalytic and antimicrobial activities of biosynthesized silver nanoparticles using Cytobacillus firmus. Life. 2022;12(9):1331. doi: 10.3390/life12091331. PMID: 36143368.

[17] Hashem AH, El-Sayyad GS. Antimicrobial and anticancer activities of biosynthesized bimetallic silver-zinc oxide nanoparticles (Ag-ZnO NPs) using pomegranate peel extract. Biomass Convers Biorefin. 2024;14(17):20345–57.

[18] El-Khawaga AM, Elsayed MA, Gobara M, Suliman AA, Hashem AH, Zaher AA, et al. Green synthesized ZnO nanoparticles by Saccharomyces cerevisiae and their antibacterial activity and photocatalytic degradation. Biomass Convers Biorefin. 2023;15:1–2.

[19] Hashem AH, Saied E, Ali OM, Selim S, Al Jaouni SK, Elkady FM, et al. Pomegranate peel extract stabilized selenium nanoparticles synthesis: promising antimicrobial potential, antioxidant activity, biocompatibility, and hemocompatibility. Appl Biochem Biotechnol. 2023;195(10):5753–76. doi: 10.1007/s12010-023-04326-y. PMID: 36705842.

[20] Saied M, Hasanin M, Abdelghany TM, Amin BH, Hashem AH. Anticandidal activity of nanocomposite based on nanochitosan, nanostarch and mycosynthesized copper oxide nanoparticles against multidrug-resistant Candida. Int J Biol Macromol. 2023;242:124709. doi: 10.1016/j.ijbiomac.2023.124709. PMID: 37141971.

[21] Saied E, Mekky AE, Al-Askar AA, Hagag AF, El-bana AA, Ashraf M, et al. Aspergillus terreus-mediated selenium nanoparticles and their antimicrobial and photocatalytic activities. Crystals. 2023;13(3):450.

[22] Hashem AH, El-Naggar ME, Abdelaziz AM, Abdelbary S, Hassan YR, Hasanin MS. Bio-based antimicrobial food packaging films based on hydroxypropyl starch/polyvinyl alcohol loaded with the biosynthesized zinc oxide nanoparticles. Int J Biol Macromol. 2023;249:126011. doi: 10.1016/j.ijbiomac.2023.126011. PMID: 37517763.

[23] Al-Askar AA, Hashem AH, Elhussieny NI, Saied E. Green biosynthesis of zinc oxide nanoparticles using Pluchea indica leaf extract: antimicrobial and photocatalytic activities. Molecules. 2023;28(12):4679. doi: 10.3390/molecules28124679. PMID: 37375234.

[24] Landage KS, Arbade GK, Khanna P, Bhongale CJ. Biological approach to synthesize TiO_2 nanoparticles using Staphylococcus aureus for antibacterial and anti-biofilm applications. J Microbiol Exp. 2020;8(1):36–43.

[25] Manna J, Begum G, Kumar KP, Misra S, Rana RK. Enabling antibacterial coating via bioinspired mineralization of nanostructured ZnO on fabrics under mild conditions. ACS Appl Mater Interfaces. 2013;5(10):4457–63. doi: 10.1021/am400933n. PMID: 23607588.

[26] Sathyanarayanan MB, Balachandranath R, Genji Srinivasulu Y, Kannaiyan SK, Subbiahdoss G. The effect of gold and iron-oxide nanoparticles on biofilm-forming pathogens. Int Sch Res Not. 2013;2013(1):272086.

[27] Hashem AH, Al-Askar AA, Haponiuk J, Abd-Elsalam KA, Hasanin MS. Biosynthesis, characterization, and antifungal activity of novel trimetallic copper oxide–selenium–zinc oxide nanoparticles against some mucorales fungi. Microorganisms. 2023;11(6):1380. doi: 10.3390/microorganisms11061380. PMID: 37374882.

[28] Basavegowda N, Baek KH. Multimetallic nanoparticles as alternative antimicrobial agents: challenges and perspectives. Molecules. 2021;26(4):912. doi: 10.3390/molecules26040912. PMID: 33572219.

[29] Gaber SE, Hashem AH, El-Sayyad GS, Attia MS. Antifungal activity of myco-synthesized bimetallic ZnO-CuO nanoparticles against fungal plant pathogen Fusarium oxysporum. Biomass Convers Biorefin. 2024;14(20):25395–409.

[30] Hasanin MS, Hashem AH, Al-Askar AA, Haponiuk J, Saied E. A novel nanocomposite based on mycosynthesized bimetallic zinc-copperoxide nanoparticles, nanocellulose and chitosan: characterization, antimicrobial and photocatalytic activities. Electron J Biotechnol. 2023;65:45–55.

[31] Skłodowski K, Chmielewska-Deptuła SJ, Piktel E, Wolak P, Wollny T, Bucki R. Metallic nanosystems in the development of antimicrobial strategies with high antimicrobial activity and high biocompatibility. Int J Mol Sci. 2023;24(3):2104. doi: 10.3390/ijms24032104. PMID: 36768426.

[32] Hameed RS, Fayyad RJ, Nuaman RS, Hamdan NT, Maliki SA. Synthesis and characterization of a novel titanium nanoparticals using banana peel extract and investigate its antibacterial and insecticidal activity. J Pure Appl Microbiol. 2019;13(4):2241–9.

[33] Kamli MR, Srivastava V, Hajrah NH, Sabir JS, Hakeem KR, Ahmad A, et al. Facile bio-fabrication of Ag-Cu-Co trimetallic nanoparticles and its fungicidal activity against Candida auris. J Fungi. 2021;7(1):62. doi: 10.3390/jof7010062. PMID: 33477480.
[34] Alshehri AA, Malik MA. Facile one-pot biogenic synthesis of Cu-Co-Ni trimetallic nanoparticles for enhanced photocatalytic dye degradation. Catalysts. 2020;10(10):1138.
[35] Nazir MA, Hasan M, Mustafa G, Tariq T, Ahmed MM, Golzari Dehno R, et al. Zinc oxide nano-fertilizer differentially effect on morphological and physiological identity of redox-enzymes and biochemical attributes in wheat (Triticum aestivum L.). Sci Rep. 2024;14(1):13091. doi: 10.1038/s41598-024-63987-9. PMID: 38849601.
[36] Sangwan S, Seth R. Synthesis, characterization and stability of gold nanoparticles (AuNPs) in different buffer systems. J Clust Sci. 2022;33:749–64. doi: 10.1007/s10876-020-01956-8.
[37] Shukla V, Niveria K, Shashidhar P, Verma AK. Dynamic light scattering (DLS) particle size analysis for biomedical nanotechnology. In Analytical Techniques for Biomedical Nanotechnology. Bristol, UK: IOP Publishing; 2023. p. 16.
[38] Perez C. Antibiotic assay by agar-well diffusion method. Acta Biol Med Exp. 1990;15:113–5.
[39] Humphries RM, Ambler J, Mitchell SL, Castanheira M, Dingle T, Hindler JA, et al. CLSI methods development and standardization working group best practices for evaluation of antimicrobial susceptibility tests. J Clin Microbiol. 2018;56(4):10–128. doi: 10.1128/JCM.01934-17. PMID: 29367292.
[40] Khattab AM, Abo-Taleb HA, Abdelaziz AM, El-Tabakh MA, El-Feky MM, Abu-Elghait M. Daphnia magna and Gammarus pulex, novel promising agents for biomedical and agricultural applications. Sci Rep. 2022;12(1):13690. doi: 10.1038/s41598-022-17790-z. PMID: 35953507.
[41] Mosmann T. Rapid colorimetric assay for cellular growth and survival: application to proliferation and cytotoxicity assays. J Immunol Methods. 1983;65(1–2):55–63. doi: 10.1016/0022-1759(83)90303-4. PMID: 6606682.
[42] Adeyemi JO, Oriola AO, Onwudiwe DC, Oyedeji AO. Plant extracts mediated metal-based nanoparticles: synthesis and biological applications. Biomolecules. 2022;12(5):627. doi: 10.3390/biom12050627. PMID: 35625555.
[43] Godeto YG, Ayele A, Ahmed IN, Husen A, Bachheti RK. Medicinal plant-based metabolites in nanoparticles synthesis and their cutting-edge applications: an overview. Secondary metabolites from medicinal plants. Vol. 2. Cham, Switzerland: Springer Nature; 2023. p. 1–34.
[44] Rangga WD, Setiawan D, Khosiatun K. Biosynthesis and kinetics of silver nanoparticles formation by reduction using banana kepok (Musa balbisiana) peel extract. ASEAN J Chem Eng. 2017;17(2):77–85.
[45] Bankar A, Joshi B, Kumar AR, Zinjarde S. Banana peel extract mediated novel route for the synthesis of palladium nanoparticles. Mater Lett. 2010;64(18):1951–3.
[46] Khan AI, Arasu AV. A review of influence of nanoparticle synthesis and geometrical parameters on thermophysical properties and stability of nanofluids. Therm Sci Eng Prog. 2019;11:334–64.
[47] Patil S, Chandrasekaran R. Biogenic nanoparticles: a comprehensive perspective in synthesis, characterization, application and its challenges. J Genet Eng Biotechnol. 2020;18(1):67. doi: 10.1186/s43141-020-00081-3. PMID: 33104931.
[48] Dlugaszewska J, Dobrucka R. Effectiveness of biosynthesized trimetallic Au/Pt/Ag nanoparticles on planktonic and biofilm Enterococcus faecalis and Enterococcus faecium forms. J Clust Sci. 2019;30:1091–101.
[49] Dobrucka R. Biogenic synthesis of trimetallic nanoparticles Au/ZnO/Ag using Meliloti officinalis extract. Int J Environ Anal Chem. 2020;100(9):981–91.
[50] Vaseghi Z, Tavakoli O, Nematollahzadeh A. Rapid biosynthesis of novel Cu/Cr/Ni trimetallic oxide nanoparticles with antimicrobial activity. J Environ Chem Eng. 2018;6(2):1898–911.
[51] Rao KJ, Paria S. Mixed phytochemicals mediated synthesis of multifunctional Ag–Au–Pd nanoparticles for glucose oxidation and antimicrobial applications. ACS Appl Mater Interfaces. 2015;7(25):14018–25. doi: 10.1021/acsami.5b03089. PMID: 26043395.
[52] Kaur M, Singh J, Chauhan M, Kumar V, Singh K. Green synthesis of TiO_2-Al_2O_3-$ZnFe_2O_4$ nanocomposite using the Hibiscus rosa sinesis and evaluation of its photocatalytic applications. Open Ceram. 2024;18:100571.
[53] Hassan H, Omoniyi KI, Okibe FG, Nuhu AA, Echioba EG. Evaluation of antibacterial potential of biosynthesized plant leave extract mediated titanium oxide nanoparticles using Hypheae thiebeace and anannos seneglensis. J Appl Sci Environ Manag. 2019;23(10):1795–804.
[54] Vergheese M, Vishal SK. Green synthesis of magnesium oxide nanoparticles using Trigonella foenum-graecum leaf extract and its antibacterial activity. J Pharmacogn Phytochem. 2018;7(3):1193–200.
[55] Hassanisaadi M, Bonjar GH, Rahdar A, Pandey S, Hosseinipour A, Abdolshahi R. Environmentally safe biosynthesis of gold nanoparticles using plant water extracts. Nanomaterials. 2021;11(8):2033. PMID: 34443864 PMCID: PMC8400837 doi: 10.3390/nano11082033.
[56] Kannaiyan SK, Rengaraj R, Gayathri PK, Lavanya G, Hemapriya D. Antimicrobial activity of green synthesized tri-metallic oxide Ni/Cr/Cu nanoparticles. J Nig Soc Phys Sci. 2021;3:144–7. doi: 10.46481/jnsps.2021.237.
[57] Hussein S, Mahmoud AM, Elgebaly HA, Hendawy OM, Hassanein EH, Moustafa SM, et al. Green synthesis of trimetallic nanocomposite (Ru/Ag/Pd)-Np and its *in vitro* antimicrobial and anticancer activities. J Chem. 2022;2022(1):4593086.
[58] Khan AU, Arooj A, Tahir K, Ibrahim MM, Jevtovic V, AL-Abdulkarim HA, et al. Facile fabrication of novel Ag_2S-ZnO/GO nanocomposite with its enhanced photocatalytic and biological applications. J Mol Struct. 2022;1251:131991.
[59] Botteon CE, Silva LB, Ccana-Ccapatinta GV, Silva TS, Ambrosio SR, Veneziani RC, et al. Biosynthesis and characterization of gold nanoparticles using Brazilian red propolis and evaluation of its antimicrobial and anticancer activities. Sci Rep. 2021;11(1):1974. PMID: 33479338 PMCID: PMC7820602. doi: 10.1038/s41598-021-81281-w.
[60] Henzie J, Grünwald M, Widmer-Cooper A, Geissler PL, Yang P. Self-assembly of uniform polyhedral silver nanocrystals into densest packings and exotic superlattices. Nat Mater. 2012;11(2):131–7. doi: 10.1038/nmat3178. PMID: 22101811.
[61] Nassar AM, Elseman AM, Alsohaimi IH, Alotaibi NF, Khan A. Diaqua oxalato strontium (II) complex as a precursor for facile fabrication of Ag-NPs@ $SrCO_3$, characterization, optical properties, morphological studies and adsorption efficiency. J Coord Chem. 2019;72(5–7):771–85.
[62] Hussien NA. Antimicrobial potential of biosynthesized zinc oxide nanoparticles using banana peel and date seeds extracts. Sustainability. 2023;15(11):9048.

[63] Canaparo R, Foglietta F, Limongi T, Serpe L. Biomedical applications of reactive oxygen species generation by metal nanoparticles. Materials. 2020;14(1):53. doi: 10.3390/ma14010053. PMID: 33374476.
[64] Sidhu AK, Verma N, Kaushal P. Role of biogenic capping agents in the synthesis of metallic nanoparticles and evaluation of their therapeutic potential. Front Nanotechnol. 2022;3:801620.
[65] Rathi VH, Jeice AR. Green fabrication of titanium dioxide nanoparticles and their applications in photocatalytic dye degradation and microbial activities. Chem Phys Impact. 2023;6:100197.
[66] Saidi NS, Ying KJ, Yusoff HM, Badar N. Synthesis and characterization of magnesium oxide nanoparticles by using banana peel (Musa Acuminata Cavendish) extract. Malay J Anal Sci. 2023;27(5):1017–34.
[67] Deokar GK, Ingale AG. Green synthesis of gold nanoparticles (Elixir of Life) from banana fruit waste extract–an efficient multifunctional agent. RSC Adv. 2016;6(78):74620–9.
[68] Said AR, Arafa MF, El-Dakroury WA, Alshehri S, El Maghraby GM. Bilosomes and niosomes for enhanced intestinal absorption and *in vivo* efficacy of cytarabine in treatment of Acute Myeloid Leukemia. Pharmaceuticals. 2024;17(12):1572. doi: 10.3390/ph17121572. PMID: 39770414.
[69] Caputo F, Vogel R, Savage J, Vella G, Law A, Della Camera G, et al. Measuring particle size distribution and mass concentration of nanoplastics and microplastics: addressing some analytical challenges in the sub-micron size range. J Colloid Interface Sci. 2021;588:401–17. doi: 10.1016/j.jcis.2020.12.039. PMID: 33422789.
[70] Roy A, Kunwar S, Bhusal U, Idris DS, Alghamdi S, Chidambaram K, et al. Dye degradation activity of biogenically synthesized Cu/Fe/Ag trimetallic nanoparticles. Green Process Synth. 2024;13(1):20230267.
[71] Xu F. Review of analytical studies on TiO_2 nanoparticles and particle aggregation, coagulation, flocculation, sedimentation, stabilization. Chemosphere. 2018;212:662–77. doi: 10.1016/j.chemosphere.2018.08.108. PMID: 30173113.
[72] Orshiso TA, Zereffa EA, Murthy HA, Demissie TB, Ghotekar S, Pagar K, et al. One-pot biopreparation of trimetallic ZnO–MgO–CuO nanoparticles: enhanced cytotoxicity, antibacterial activities and molecular docking studies. Chem Afr. 2024;7(4):1963–80. doi: 10.1007/s42250-023-00830-0.
[73] Nguyen TT, Nguyen YN, Tran XT, Nguyen TT, Van Tran T. Green synthesis of CuO, ZnO and CuO/ZnO nanoparticles using Annona glabra leaf extract for antioxidant, antibacterial and photocatalytic activities. J Environ Chem Eng. 2023;11(5):111003.
[74] Haque B, Gupta A, Roy A, Malik A, Khan AA. Green fabrication of Ag–Ni–Mn-Zn nanoparticles from watermelon peels and its antioxidant, dye degradation and molecular docking studies. Clean Technol Environ Policy. 2024;7:1–28.
[75] Cai L, Chen J, Liu Z, Wang H, Yang H, Ding W. Magnesium oxide nanoparticles: effective agricultural antibacterial agent against Ralstonia solanacearum. Front Microbiology. 2018;9:790. doi: 10.3389/fmicb.2018.00790. PMID: 29922237.
[76] Noori AJ, Kareem FA. The effect of magnesium oxide nanoparticles on the antibacterial and antibiofilm properties of glass-ionomer cement. Heliyon. 2019;5(10):e02568. doi: 10.1016/j.heliyon.2019.e02568. PMID: 31667407.
[77] Shkodenko L, Kassirov I, Koshel E. Metal oxide nanoparticles against bacterial biofilms: Perspectives and limitations. Microorganisms. 2020;8(10):1545. doi: 10.3390/microorganisms8101545. PMID: 33036373.
[78] Sharma G, Soni R, Jasuja ND. Phytoassisted synthesis of magnesium oxide nanoparticles with Swertia chirayaita. J Taibah Univ Sci. 2017;11(3):471–7.
[79] Ekielski A. Interactions between food ingredients and nanocomponents used for composite packaging. In: Grumezescu AM, Holban AM, editors. Food packaging and preservation. London, UK: Academic Press; 2019. p. 669–74.
[80] Behzad F, Naghib SM, Tabatabaei SN, Zare Y, Rhee KY. An overview of the plant-mediated green synthesis of noble metal nanoparticles for antibacterial applications. J Ind Eng Chem. 2021;94:92–104.
[81] Ortiz-Benítez EA, Velázquez-Guadarrama N, Durán Figueroa NV, Quezada H, Olivares-Trejo JD. Antibacterial mechanism of gold nanoparticles on Streptococcus pneumoniae. Metallomics. 2019;11(7):1265–76. doi: 10.1039/c9mt00084d. PMID: 31173034.
[82] Lee NY, Ko WC, Hsueh PR. Nanoparticles in the treatment of infections caused by multidrug-resistant organisms. Front Pharmacol. 2019;10:1153. doi: 10.3389/fphar.2019.01153. PMID: 31636564.
[83] Varier KM, Gudeppu M, Chinnasamy A, Thangarajan S, Balasubramanian J, Li Y, et al. Nanoparticles: antimicrobial applications and its prospects. Advanced nanostructured materials for environmental remediation. Amsterdam, Netherlands: Elsevier; 2019. p. 321–55. doi: 10.1007/978-3-030-04477-0_12.
[84] Spirescu VA, Chircov C, Grumezescu AM, Andronescu E. Polymeric nanoparticles for antimicrobial therapies: An up-to-date overview. Polymers. 2021;13(5):724. doi: 10.3390/polym13050724. PMID: 33673451.
[85] Baig U, Ansari MA, Gondal MA, Akhtar S, Khan FA, Falath WS. Single step production of high-purity copper oxide-titanium dioxide nanocomposites and their effective antibacterial and anti-biofilm activity against drug-resistant bacteria. Mater Sci Eng: C. 2020;113:110992. doi: 10.1016/j.msec.2020.110992. PMID: 32487404.
[86] N Oktar F, Yetmez M, Ficai D, Ficai A, Dumitru F, Pica A. Molecular mechanism and targets of the antimicrobial activity of metal nanoparticles. Curr Top Med Chem. 2015;15(16):1583–8. doi: 10.2174/1568026615666150414141601. PMID: 25877090.
[87] Khan F, Manivasagan P, Lee JW, Pham DT, Oh J, Kim YM. Fucoidan-stabilized gold nanoparticle-mediated biofilm inhibition, attenuation of virulence and motility properties in Pseudomonas aeruginosa PAO1. Mar Drugs. 2019;17(4):208. doi: 10.3390/md17040208. PMID: 30987163.
[88] Samanta S, Singh BR, Adholeya A. Intracellular synthesis of gold nanoparticles using an ectomycorrhizal strain EM-1083 of Laccaria fraterna and its nanoanti-quorum sensing potential against Pseudomonas aeruginosa. Indian J Microbiol. 2017;57:448–60. doi: 10.1007/s12088-017-0662-4. PMID: 29151646.
[89] Anwar A, Perveen S, Ahmed S, Siddiqui R, Shah MR, Khan NA. Silver nanoparticle conjugation with thiopyridine exhibited potent antibacterial activity against Escherichia coli and further enhanced by copper capping. Jundishapur J Microbiol. 2019;12(3):e74455. doi: 10.5812/jjm.74455.
[90] Aljaafari A, Ahmed F, Husain FM. Bio-inspired facile synthesis of graphene-based nanocomposites: elucidation of antimicrobial and biofilm inhibitory potential against foodborne pathogenic bacteria. Coatings. 2020;10(12):1171.

[91] Rajkumari J, Magdalane CM, Siddhardha B, Madhavan J, Ramalingam G, Al-Dhabi NA, et al. Synthesis of titanium oxide nanoparticles using Aloe barbadensis mill and evaluation of its antibiofilm potential against Pseudomonas aeruginosa PAO1. J Photochem Photobiol B: Biol. 2019;201:111667. doi: 10.1016/j.jphotobiol.2019.111667. PMID: 31683167.

[92] Achudhan D, Vijayakumar S, Malaikozhundan B, Divya M, Jothirajan M, Subbian K, et al. The antibacterial, antibiofilm, antifogging and mosquitocidal activities of titanium dioxide (TiO_2) nanoparticles green-synthesized using multiple plants extracts. J Environ Chem Eng. 2020;8(6):104521.

[93] Younis IY, El-Hawary SS, Eldahshan OA, Abdel-Aziz MM, Ali ZY. Green synthesis of magnesium nanoparticles mediated from Rosa floribunda charisma extract and its antioxidant, antiaging and antibiofilm activities. Sci Rep. 2021;11(1):16868. doi: 10.1038/s41598-021-96377-6. PMID: 34413416.

[94] Sivasubramanian K, Tamilselvi Y, Velmurugan P, Al-Otibi FO, Alharbi RI, Mohanavel V, et al. Enhanced applications in dentistry through autoclave-assisted sonochemical synthesis of Pb/Ag/Cu trimetallic nanocomposites. Ultrason Sonochem. 2024;22:106966. doi: 10.1016/j.ultsonch.2024.106966. PMID: 38924854.

[95] Garza-Cervantes JA, Escárcega-González CE, Barriga Castro ED, Mendiola-Garza G, Marichal-Cancino BA, López-Vázquez MA, et al. Antimicrobial and antibiofilm activity of biopolymer-Ni, Zn nanoparticle biocomposites synthesized using R. mucilaginosa UANL-001L exopolysaccharide as a capping agent. Int J Nanomed. 2019;10:2557–71. doi: 10.2147/IJN.S196470. PMID: 31118605.

[96] Lotfian H, Nemati F. Cytotoxic effect of TiO_2 nanoparticles on breast cancer cell line (MCF-7). IIOAB J. 2016;7:219–24.

[97] Guo M, Sun Y, Zhang XD. Enhanced radiation therapy of gold nanoparticles in liver cancer. Appl Sci. 2017;7(3):232.

[98] Gong L, Tang Y, An R, Lin M, Chen L, Du J. RTN1-C mediates cerebral ischemia/reperfusion injury via ER stress and mitochondria-associated apoptosis pathways. Cell Death Dis. 2017;8(10):e3080. doi: 10.1038/cddis.2017.465. PMID: 28981095.

[99] Onodera R, Jimma Y, Suzuki A, Habano W, Ozawa S, Terashima J. The regulation pathway of VEGF gene expression is different between 2D cells and 3D spheroids in human lung cancer cells. Biol Pharm Bull. 2023;46(4):608–13. doi: 10.1248/bpb.b22-00772. PMID: 37005305.

[100] Amirchaghmaghi E, Rezaei A, Moini A, Roghaei MA, Hafezi M, Aflatoonian R. Gene expression analysis of VEGF and its receptors and assessment of its serum level in unexplained recurrent spontaneous abortion. Cell J (Yakhteh). 2015;16(4):538. doi: 10.22074/cellj.2015.498. PMID: 25685744.

[101] Pochapski DJ, Carvalho dos Santos C, Leite GW, Pulcinelli SH, Santilli CV. Zeta potential and colloidal stability predictions for inorganic nanoparticle dispersions: Effects of experimental conditions and electrokinetic models on the interpretation of results. Langmuir. 2021;37(45):13379–89. doi: 10.1021/acs.langmuir.1c02056.

[102] Sharma D, Kanchi S, Bisetty K. Biogenic synthesis of nanoparticles: a review. Arab J Chem. 2019;12(8):3576–600. doi: 10.1016/j.arabjc.2015.11.002.

[103] Mahmood K, Amara U, Siddique S, Usman M, Peng Q, Khalid M, et al. Green synthesis of Ag@ CdO nanocomposite and their application towards brilliant green dye degradation from wastewater. J Nanostruct Chem. 2022;12:329–41. doi: 10.1007/s40097-021-00418-5.

[104] Karvekar OS, Sarvalkar PD, Vadanagekar AS, Singhan RD, Jadhav SM, Nimbalkar MS, et al. Biogenic synthesis of silver anchored ZnO nanorods as nano catalyst for organic transformation reactions and dye degradation. Appl Nanosci. 2022;12(7):2207–26. doi: 10.1007/s13204-022-02470-1.

[105] El-Sawaf AK, El-Moslamy SH, Kamoun EA, Hossain K. Green synthesis of trimetallic CuO/Ag/ZnO nanocomposite using Ziziphus spina-christi plant extract: characterization, statistically experimental designs, and antimicrobial assessment. Sci Rep. 2024;14(1):19718. doi: 10.1038/s41598-024-67579-5.